UNIVERSITA' DEGLI STUDI DI VERONA

DIPARTIMENTO DI MEDICINA

SCUOLA DI DOTTORATO DI

SCIENZE DELLA VITA E DELLA SALUTE

DOTTORATO DI RICERCA IN

INFIAMMAZIONE, IMMUNITA' E CANCRO

CICLO /ANNO XXXI/2015

TITOLO DELLA TESI DI DOTTORATO

Histogram analysis of magnetic resonance images: evaluation of intra-tumoral heterogeneity and correlation with pathological findings in solid pancreatic tumors.

S.S.D. MED/36

Coordinatore: Prof.ssa Gabriela Constantin

Tutor: Prof. Davide Melisi

Dottorando: Dott. Riccardo De Robertis Lombardi

Histogram analysis of magnetic resonance images: evaluation of intra-tumoral heterogeneity and correlation with pathological findings in solid pancreatic tumors

.

Riccardo De Robertis Lombardi

Tesi di Dottorato

Verona, 6/5/2019

Abstract

Objectives

To evaluate magnetic resonance (MR)-derived whole-tumor histogram analysis parameters in predicting aggressiveness of pancreatic ductal adenocarcinomas (PDACs) and neuroendocrine neoplasms (panNENs).

Methods

Pre-operative MR of 169 consecutive patients with PDAC or panNEN were retrospectively analyzed. T1-/T2-weighted images and apparent diffusion coefficient (ADC) maps were analyzed. Histogram-derived parameters were compared to several pathological features (grade, vascular infiltration, nodal and hepatic metastases) using Mann-Whitney U test. Diagnostic accuracy was assessed by receiver operating characteristic area under curve (ROC-AUC) analysis; sensitivity and specificity were assessed for each histogram parameter.

Results

No significant differences were found among histogram parameters for prediction of PDACs grade. $ADC_{entropy}$ was significantly higher in G2-3 panNENs with ROC-AUC 0.757; sensitivity was 83.3%. $ADC_{entropy}$ was significantly higher in PDACs with vascular involvement (p=.022; AUC=.641), with specificity of 92.2%. $ADC_{skewness}$ was significantly higher in PDACs with nodal metastases (p=.027; AUC=.642), with 72% specificity. $ADC_{kurtosis}$ was higher in panNENs with vascular involvement, nodal and hepatic metastases (p= .008, .021, and .008; ROC-AUC= 0.820, 0.709, and 0.820); sensitivity and specificity were: 85.7/74.3%; 36.8/96.5%; and 100/62.8%. No significant differences between groups were found for other histogram-derived parameters (p >.05).

Conclusions

Whole-tumors histogram analysis of ADC values is a valuable tool for predicting aggressiveness of PDACs and panNENs. Our results indicate that histogram metrics related to intra-tumor heterogeneity, as $ADC_{entropy}$, $ADC_{kurtosis}$ and

$ADC_{skewness}$ are the most accurate parameters for the identification of PDACs and panNENs with higher biological aggressiveness. Further and larger studies are needed to incorporate the results of the histogram analysis within decision support models and to mine these data to detect possible correlations with genomic patterns.

Summary

1. Introduction

a) Epidemiology, pathology and molecular/genomic landscape of solid pancreatic tumors

Pancreatic tumors arise from both the exocrine and endocrine parenchyma of the gland; however, about 95% occur within the exocrine portion and may arise from ductal epithelium, acinar cells, or connective tissue, and only 2% of these exocrine tumors are benign. The most common solid pancreatic malignancy is ductal adenocarcinoma (PDAC), accounting for about 80% of all pancreatic cancers. Pancreatic adenocarcinoma represents the fourth cause of cancer death in Europe in both genders, after lung, colorectal, and prostate cancers in men, and after breast, colorectal and lung cancers in women [1]. The mortality rate of PDAC in Europe has increased by around 20% over the last 10 years [1]; incidence and mortality rates are very similar, due to the dismal prognosis of this tumor, with a life expectancy of about 5% at 5 years, that has not significantly improved over the last 20 years [1]. The mean age at diagnosis is 71 and 75 years in men and women, respectively. The vast majority (>80%) of PDACs are caused by sporadic occurring genetic alterations. The most relevant acquired risk factors for PDAC are cigarette smoking (overall relative risk, ORR, 1.74) and obesity (body mass index (BMI) > 30 kb/m^2), which is associated with an increase by 20-40% of death from pancreatic cancer. Other risk factors include diabetes (ORR for type 1 and type 2 diabetes: 2.0 and 1.8, respectively) and chronic pancreatitis, that most commonly depends, in Europe, by alcohol consumption, which is itself considered a risk factor for pancreatic cancer [2]. Additionally, Helicobacter pylori, hepatitis B and human immunodeficiency virus infection have been associated with an increase in relative risk of pancreatic cancer [2]; between dietary factors, regardless of their role in causing obesity, butter, saturated fat, red meat, and processed foods are considered risk factors for pancreatic cancer, whereas a high fruit and folate intake may have a protective role [3]. Finally, many chemical substances (such as chlorobenzoil, chlorinated hydrocarbon, nickel and nickel compounds, chromium compounds, silica dust), have been reported to increase the relative risk of developing pancreatic

cancer [4]. About 5-10% of PDACs are caused by inherited germline mutations [2], and are defined familial PDACs; this condition should be suspected and investigated when at least two first-degree relatives have been diagnosed with pancreatic cancer. Mutation in BRCA2 is the most common known inherited disorder in familial PDAC; germline mutation in other genes, such as p16, ATM, STK11, PRSS1/PRSS2, SPINK1, PALB2, and DNA mismatch repair genes, are associated with pancreatic cancer risk increase [2]. About two thirds of PDACs (60-70%) arise in the head of the pancreas, 20-25% in the body and in the tail, and 10-20% diffusely involve the pancreas. Early symptoms are strictly connected with the tumor position within the gland: pancreatic head tumors often present with "mass effect" symptoms, such as jaundice or upper gastroduodenal obstruction due to compression/invasion of the common bile and/or the pancreatic duct or the duodenum; body-tail tumors are generally associated with non-specific symptoms, such as abdominal or back pain, weight loss, steatorrhea, and new-onset diabetes [5]. Surgical resection is the only potentially curative treatment, leading to a post-operative 5-year survival rate of about 20%. Unfortunately, only 15-20% of patients present with resectable disease at diagnosis, whereas most patients present with PDAC in an advanced stage, that ranges from inoperable, locally advanced to metastatic disease. The best treatment strategy in each patient needs to be discussed by a multidisciplinary team in order to define treatment goals and possible ways to achieve them. Locally advanced tumors, defined as neoplasms with no evidence of distant metastases but that are not resectable nor borderline resectable, have an intermediate prognosis: median overall survival range from 9-12 months in untreated patients to 16 months in patients treated with active chemotherapy [6]. Chemoradiation is another option in this subgroup; however, it remains unclear whether the addiction of radiotherapy leads to superior survival compared to chemotherapy alone [6-11]. In the metastatic setting, the main treatment goal is palliation. For patients with good performance status (ECOG 0-1), adequate biliary drainage and liver function, lengthening of survival is another possible purpose, that may be pursued through the use of systemic therapy [12]; however, even with the use of polychemotherapy, the prognosis remains poor, with a median OS of 7 to 11 months according to the treatment received [13,14]. Macroscopically, PDAC

usually presents as solid, firm mass, with ill-defined margins. Microscopically, PDACs are characterized by an intense stromal reaction surrounding tumor cells [15]; these may vary from well-differentiated, duct-forming tumor cells, to poorly differentiated cells, with epithelial differentiation demonstrable only on immunolabelling. Morphological variants of PDAC include colloid carcinoma, medullary carcinoma, acinar cell pancreatic cancer (with slightly better prognosis), adenosquamous carcinoma and undifferentiated carcinomas with osteoclast-like giant cells, the last two associated with a poorer prognosis [16]. Most PDACs originate from a precursor lesion called pancreatic intraepithelial neoplasia (PanIN), a microscopic (<5mm) mucinous-papillary lesion that evolve to invasive carcinoma through an adenoma-carcinoma sequence [17]. Other potential precursor lesions are IPMNs and mucinous cystic neoplasms, that can also lead to invasive PDAC by stepwise gene alterations. Multiple genetic alterations are commonly found in PDACs: mutational activation of oncogenes (predominantly KRAS, found in >90% of PDACs), inactivation of tumor suppressor genes (such as TP53, p16/CDKN2A, and SMAD4), and inactivation of DNA damage repair genes (such as hMLH1 and MSH2) [18]. A recent whole-genome sequencing and copy number variation analysis [19] found chromosomal rearrangements as the most common event, causing disruption of genes involved in pancreatic cancer initiation and progression (TP53, SMAD4, CDKN2A, ARID1A, ROBO2, KDM6A and PREX2). According to the patterns of structural variation in chromosomes, a classification of PDACs into four subtypes with potential clinical utility has been proposed: stable, locally rearranged, scattered, and unstable subtype [20].

Pancreatic neuroendocrine neoplasms (panNENs) are the second most frequent tumor type arising in the pancreas. Neuroendocrine neoplasms (NENs) are classified according to their site of origin, their proliferation index and their functional status. The main division depending on NENs proliferation index (ki67%) is between well and poorly differentiated tumors, with the former being grouped together as grade 1 (ki67 < 3%) and grade 2 (ki67 2-20%) neuroendocrine tumor (NETs) and the latter being described as grade 3 (ki67 > 20%) neuroendocrine carcinomas (NECs) [20]. Recently, however, it has been pointed out that that within these groups there is significant heterogeneity of behavior, and

further subdivisions (i.e. highly proliferative but better differentiated tumors with a Ki-67 of <50% and truly poorly differentiated tumors with Ki-67 of >50%) may be useful to achieve better prognostic and predictive results [21]. According to the functional status, NENs are described as functional when signs and symptoms consistent with excess hormone secretion are found, regardless of hormone staining on immunohistochemical testing [22]. Insulinomas are the most common subtype of functioning PanNET, with an annual incidence of 0.5/100000 [23]. Insulinomas are usually smaller than 2 cm, solitary, hypervascular, and tend to exhibit very low malignant potential. The clinical presentation of insulinomas is characterized by the classic "Whipple triad," consisting of symptomatic hypoglycemia, low blood glucose levels, and relief of symptoms after glucose administration [24]. Gastrinomas are typically malignant tumors and cause the Zollinger-Ellison syndrome, which is characterized by peptic ulceration, heartburn, and diarrhea [25]. Vasoactive intestinal polypeptide (VIP) stimulates intestinal secretion and inhibits electrolyte and water absorption: consequently, VIPomas are associated with profuse, watery diarrhea and electrolyte abnormalities, including hypokalemia (Verner-Morrison syndrome) [26]. The clinical manifestations of glucagonomas include hyperglycemia, weight loss, venous thromboses, glossitis, and an unusual rash called necrolytic migratory erythema, likely caused by amino-acid or zinc deficiencies [27]. Somatostatinomas are characterized by the effects of hypersecretion of somatostatin and usually present with steatorrhea, achlorhydria, diabetes mellitus, and cholelithiasis. Rarely, pNETs may secrete adrenocorticotropic hormone, parathyroid hormone-related peptide, growth hormone-releasing hormone, cholecystokinin, and serotonin, giving rise to the respective clinical syndromes [28]. However, most (60-90% in recent series) PanNENs are silent hormonally, therefore defined as "non-functioning" (NF Pan-NENs) [29]; additionally, most PanNENs are well to moderately differentiated (G1-2 NETs) rather than NECs, with a relatively indolent behavior [30,31]. The crude annual incidence of NF PanNENs is 1.8 in females and 2.6 in males; their relatively good prognosis lead to a higher prevalence [30,32], although NF PanNENs seem to have worse prognosis compared with functioning tumors, probably as result of late diagnosis. In fact, NF-PanNENs usually become clinically apparent when they

reach a size that causes compression or invasion of adjacent organs, or when they metastasize: the most common presenting symptoms are abdominal pain (35–78%), weight loss (20–35%), anorexia and nausea (45%), whereas less frequent signs are intra-abdominal hemorrhage (4–20%), jaundice (17–50%) or a palpable mass (7–40%) [33-37]. According to SEER data [32], localized, regional, and distant stages corresponded to 14, 23, and 54% of cases, respectively. Median overall survival for patients with NF PanNENs ranges between 23 months of patients with metastatic disease to 70 and 124 of those with locoregional and localized disease, respectively [32]. Beyond stage, tumor grade is the main prognostic factor [38-40]: patients with G2 and G3 neoplasms have a respective 2- and 10-fold higher risk of death [41]. The only known risk factor for PanNENs development is the presence of specific hereditary syndromes, such as Multiple Endocrine Neoplasia Type 1 (MEN-1), Von Hippel-Lindau Disease (VHL) and Tuberous Sclerosis (TS) [29]. Although only a small number of patients with PanNENs have MEN-1 syndrome, these neoplasms occur in the 19% of patients diagnosed with MEN1 with an incidence of 3, 34 and 53% of patients at age 20, 50, and 80 years [42]. The incidence of PanNENs in VHL syndrome, instead, ranges from 11 to 17% [43,44]; NENs in VHL have a good prognosis although a small fraction of patients have an aggressive disease. Microscopically, most NF-NENs are well-differentiated tumors consisting of small, monomorphic cells arranged in islets or trabeculae with a "salt-and-pepper" chromatin pattern. Conversely, poorly differentiated tumors are often characterized as sheets of pleomorphic cells with extensive necrosis [22]. Immunohistochemical markers of neuroendocrine differentiation include synaptophysin, chromogranin A (CgA), neuron-specific enolase (NSE), and cluster of differentiation 56 (CD56) (neural cell adhesion molecule). [22]. As NETs arising in other organs, PanNETs are characterized by high-density expression of somatostatin receptors (SSTRs) [45]; well-differentiated NETs express SSTRs at an increased frequency and higher levels compared with poorly differentiated NECs. Aberrant activation of signaling by the mammalian target of rapamycin (mTOR) is a hallmark of NETs, regardless of primary site; mTOR modulates cell survival and proliferation, angiogenesis, and metabolism, and mutations in the mTOR pathway are observed in approximately 15% of pNETs [46,47]. NETs are among the most vascularized cancers: tumor

neoangiogenesis has been identified as a key event in NET progression, associated with overexpression of proangiogenic factors, including vascular endothelial growth factor (VEGF), fibroblast growth factor, platelet-derived growth factor (PDGF), and their receptors [48,49]. From a genomic point of view, in PanNETs, losses of genetic material have been described more often than chromosomal gains [50] a whole-genome sequencing study of 102 primary pNETs identified 4 signaling pathways commonly dysregulated in such tumors: 1) DNA damage repair; 2) chromatin remodeling; 3) telomere maintenance; and 4) mTOR activation. A higher than expected proportion of germline mutations has been demonstrated in clinically sporadic pNETs with mutations of the genes mutY homolog (*MUTYH*), checkpoint kinase 2 (*CHEK2*), and *BRCA2* recurring in 11% of patients [47]. Surgery represents the treatment of choice for localized PanNENs since it is associated with significant benefits in terms of survival [51]. Nevertheless, the improvement of cross-sectional imaging techniques significantly increased the detection of small NF-NET and it is now debated if all the small (< 2 cm) and asymptomatic lesions should be routinely resected [52], since most of neoplasms < or = 2 cm are likely benign or intermediate-risk lesions and only 6% of NF pancreatic NETs < or = 2 cm are malignant when incidentally discovered [53]. The choice of the appropriate management of these small tumors should be well balanced with the short- and long-term sequelae of pancreatic resection procedures, and a 'watchful-waiting' strategy could be a reasonable first approach. Many therapeutic options are available for advanced PanNENs, and again, the optimal treatment strategy (and the optimal sequence of therapies) should be discussed by an expert multidisciplinary board, taking into consideration the final treatment goal. Of course, in patients with functioning tumors, palliation of hormonal symptoms is the priority. Somatostatin is a hypothalamic hormone with wide exocrine, endocrine, paracrine, and autocrine inhibitory effects. Synthetic somatostatin analogues (SSAs) octreotide and lanreotide bind with high affinity to $SSTR_2$ and with moderate affinity to $SSTR_5$, inducing rapid palliation of symptoms in around 90% of patients with carcinoid syndrome, VIPoma and glucagonoma [45,54]. SSAs also are effective in palliating symptoms in patients with gastrinoma, although high-dose proton pump inhibitors may be even more essential in

controlling the gastric acid overproduction. Patients with advanced insulinoma respond poorly to SSAs, likely because of low expression of $SSTR_2$ by these tumors. Besides symptoms management, inhibition of tumor growth is another, fundamental treatment goal. SSAs have a role also in this setting, leading to a significant improvement in progression free survival (PFS) and overall survival (OS) in patients with well differentiated panNETs [55,56]; other potential therapies include radiolabeled somatostatin analogs (PRRT) [22], targeted therapies such as everolimus [57] and sunitinib [58], but also chemotherapy and locoregional treatments (i.e. transarterial embolization, TAE, or transarterial chemoembolization, TACE, cytoreductive surgery and liver transplant in selected cases) [22]. Data to guide the best selection of treatment after progression of disease on SSAs are scarce; randomized studies comparing active drugs are needed to provide additional data on the appropriate sequencing of treatments.

b) Imaging

Pancreatic ductal adenocarcinoma usually presents as a solid mass with infiltrative and ill-defined margins, causing ductal obstruction with secondary dilation of the main pancreatic duct and -when located in the pancreatic head- also of the common bile duct ("double-duct sign"). Pancreatic carcinoma is usually hypoechoic on B-mode ultrasound (US), hypo- or isodense on unenhanced computed tomography (CT), hypointense on T1-weighted images and with a variable appearance on T2-weighted images of magnetic resonance (MR) imaging. On contrast-enhanced examinations, PDAC is characterized by a hypoenhancing appearance, especially during the arterial phase. On delayed phase of CT and MR examinations, PDAC may present a mild pooling of contrast media with a slightly hyperdense/-intense appearance, owing to contrast medium retention within desmoplastic fibrosis [59].
Neuroendocrine neoplasms have a wide range of possible imaging appearances. They usually present as solid masses with well-defined margins, variably associated with dilation of the main pancreatic duct and the common bile duct. Larger tumors frequently present an inhomogeneous appearance, with coexistence of viable tumor tissue, necrosis, calcifications, etc. Neuroendocrine tumors are usually hypoechoic on B-mode US, hypo- or isodense on unenhanced CT, hypointense on T1-weighted images and hyperintense on T2-weighted images of MR imaging. On contrast-enhanced examinations, panNENs are typically hyperenhancing during the arterial phase; contrast medium retention over time may be present [60].
Diffusion-weighted imaging (DWI) is a relatively recent technical improvement of MR imaging which has an established role in the evaluation of pancreatic diseases. DW sequence can evaluate the diffusion of water molecules (the so-called Brownian motions) within biological tissues: all factors that narrow the extracellular compartment or modify water exchanges through cell membranes lead to an impairment of the diffusion of water molecules, that can be identified by DWI. Tissues with restriction of water diffusion present high signal intensity on DW images and low signal intensity on the apparent diffusion coefficient (ADC) map; diffusion restriction can be also quantified through the calculation of the ADC value within specific regions of interest (ROIs).

DWI appears to be a promising adjunct for the identification of solid pancreatic tumors and for the diagnosis of liver metastases. For example, a previous study [61] reported that b800 DWI images provides higher conspicuity of
panNENs compared to conventional MR sequences, thus leading to higher detection rates (93.3 vs. 71%): a probable explanation is that DW images have a high contrast resolution thanks to the decay of the MR signal of the pancreas and the peripancreatic structures on high b-value images, while pancreatic tumors, including panNENs, usually present diffusion restriction, with preservation of the MR signal, owing to the coexistence of dense cellularity, fibrosis and structural rearrangement that lead to an impaired diffusion of water molecules. As a consequence, both visual analysis and quantification of the conspicuity on high-b-value DW images will provide a better identification of these tumors. Nevertheless, previous studies have reported controversial results regarding the performance of DWI in terms of the detection of panNENs: a small study conducted by Bakir et al [62], comprising 12 panNENs, reported that DWI does not appear to add useful additional information to a routine MR imaging protocol in the evaluation of panNENs, as the detection rates with DWI and conventional sequences were similar (100 and 91.7%, respectively); nevertheless, the authors of this study concluded that in patients with clinical suspicion for panNENs with negative or doubtful imaging modality outcomes, DWI may provide ancillary findings to the routine abdominal MR examination. Some other authors suggested that DWI findings might increase the diagnostic accuracy of conventional MR sequences. Brenner et al [63] reported that the addition of postprocessed fusion images of T2 and b1000 DW images when reading MR studies of panNENs significantly increased the agreement on and confidence in the diagnosis of this neoplasia. A study by Schmid-Tannwald et al [64] reported that the detection rate with conventional MR sequences was significantly improved by the addition of DW images, increasing it from 24.8–39.1 to 60.9–65.2%. Previous studies reported that DWI may provide ancillary findings that might be useful for prognostication. Prognosis in patients with PDAC is partially influenced by the histopathologic grade; ideally, well-differentiated PDACs should present higher ADC values as compared to low-grade tumors, but some authors reported opposite findings as well as non-significant

results. It is reasonable to believe that the main contribution to the restriction of water diffusion in PDACs is provided by fibrosis, which is the predominant part of this tumor, while the contribution of the cells - even if less differentiated - and the perfusion effect provided by blood vessels should be minimal. Wang et al [65] reported that PDACs containing dense fibrosis had significantly lower ADC values compared to those characterized by abundant neoplastic tubular structures; moreover, well/moderately differentiated PDACs with dense fibrosis showed also significantly lower ADC values than those with loose fibrosis. Muraoka et al [66] reported similar findings: the mean ADC value was significantly higher in PDACs with loose fibrosis ($1.88\pm 0.39 \times 10^{-3}$ mm^2/s) than in those with dense fibrosis ($1.01 \pm 0.29 \times 10^{-3}$ mm^2/s, $p<.05$). On the other hand, Rosenkrantz et al [67] did not report significant difference in mean ADC between poorly and well/moderately differentiated tumors. Moreover, Legrand et al [68] reported that mean ADC values did not differ significantly between tumors having < 50% of fibrotic stroma and those having >50% of fibrotic stroma (p=.94), or between tumors containing dense fibrosis and those containing loose fibrosis (p=.81). Some authors have proposed a more practical role for DWI, testing correlations with clinical features or outcomes (e.g., tumor stage, aggressiveness, or survival) rather than the histopathologic grade. Hayano et al [69] reported a significant negative correlation between ADC and tumor size (r=-0.59, p=.004) and the number of metastatic lymph nodes (r=-0.56, p=.007). Tumors with low ADC values had a significant higher tendency to show portal system and extra-pancreatic nerve plexus invasion (p=.04 and .01, respectively) than those with high ADC. On the contrary, Rosenkrantz et al [67] did not report significant difference in mean ADC between tumors with stage T3 vs stage T1/T2, or between tumors with and without metastatic peri-pancreatic lymph nodes. Fukukura et al [70] reported that the median ADC value of PDACs was not associated with significantly differences in survival. Several studies identified predictors of aggressiveness by comparing DW and pathological features of panNENs, which could be helpful in the prognostication of these tumors. For instance, Lotfalizadeh et al [71] and Guo et al [72] reported that the mean ADC value tends to decrease as tumor grade increases. Similar results were reported by another study [73], which also reported an inverse correlation between the mean

ADC and tumor stage. Basing on these results, ADC seems to be correlated with aggressiveness in panNENs.

c) Radiomics and radiogenomics

The suffix -omics originated in molecular biology disciplines to describe the detailed characterization of biologic molecules such as DNA (genomics), RNA (transcriptomics), proteins (proteomics), and metabolites (metabolomics). Now, the term is also being used in other medical research fields that generate complex high-dimensional data from single objects or samples. One desirable characteristic of -omics data is that these data are mineable and, as such, can be used for exploration and hypothesis generation. The term radiomics describes the conversion of digital medical images into mineable high-dimensional data, and it is motivated by the concept that biomedical images contain information that reflects underlying pathophysiology and that these relationships can be revealed via quantitative image analyses.

Radiomics is a process designed to extract a large number of quantitative features from digital images (density/intensity, shape, size/volume, texture, etc.) which offer information on tumor phenotype and microenvironment, place these data in databases, and subsequently mine the data for hypothesis generation and/or testing. The final objective of radiomics is to develop decision support tools; therefore, it involves combining radiomic data with other tumor and patient characteristics (aggressiveness, biological behavior, survival, etc.) to increase the power of the decision support models. Radiomics appears to offer a nearly limitless supply of imaging biomarkers that could potentially aid cancer detection, diagnosis, assessment of prognosis, prediction of response to treatment, and monitoring of disease status [74].

The mining of radiomic data to detect correlations with genomic patterns is known as radiogenomics, and it has elicited great interest in the research community. The value of radiogenomics stems from the fact that while virtually all patients with cancer undergo imaging at some point and often multiple times during their care, not all of them have their disease genomically profiled. Furthermore, when genomic profiling is performed, it is done one time at one location and is susceptible to sampling error. Thus, radiogenomics has two potential uses. First, a subset of the radiomic data can be used to suggest gene expression or mutation status that

potentially warrants further testing. This is important because the radiomic data are derived from the entire tumor rather than from just a sample. Thus, radiomics can provide important information regarding the sample genomics and can be used for cross-validation. Second, a subset of radiomic features is not significantly related to gene expression or mutational data and, hence, has the potential to provide additional, independent information. The combination of this subset of radiomic features with genomic data may increase diagnostic, prognostic, and predictive power.

While radiomics primarily grew out of basic research, lately it has also elicited interest from those in clinical research, as well as those in daily clinical practice. For example, visualization of tumor heterogeneity may prove critical in the assessment of tumor aggressiveness and prognosis. For example, research has already shown the capacity of radiomics analyses to help distinguish prostate cancer from benign prostate tissue or add information about prostate cancer aggressiveness [75]. In the evaluation of lung cancer, radiomics has been shown to be a tool with which to assess patient prognosis [76]. Therefore, radiomics offers important advantages for assessment of tumor biology. It is now appreciated that most clinically relevant solid tumors are highly heterogeneous at the phenotypic, physiologic, and genomic levels [77-79] and that they continue to evolve over time. Genomic heterogeneity within tumors and across metastatic tumor sites in the same patient is the major cause of treatment failure and emergence of therapy resistance [80]. Thus, precision medicine requires not only in vitro biomarkers and companion diagnostics but also spatially and temporally resolved in vivo biomarkers of tumor biology. A central hypothesis driving radiomics research is that radiomics has the potential to enable quantitative measurement of intra- and intertumoral heterogeneity. Moreover, radiomics offers the possibility of longitudinal use in treatment monitoring and optimization or in active surveillance.

The tools developed for radiomics can help in daily clinical work, and radiologists can play a pivotal role in continuously building the databases that are to be used for future decision support. Radiomics analyses epitomize the pursuit of precision medicine, in which molecular and other biomarkers are used to predict the right treatment for the right patient at the right time. The availability of robust and

validated biomarkers is essential to move precision medicine forward. A major strength of a radiomics approach for cancer is that digital radiologic images are obtained for almost every patient with cancer, and all of these images are potential sources for radiomics databases. In the future, it is possible that image interpretation for all these studies will be augmented by using radiomics, building an unprecedented source of big data that will expand the potential for discovering helpful correlations. While radiomics will allow better characterization of patients and their diseases through new applications of genomics and improved methods of phenotyping, it will also add to the challenges of data management, as we will discuss later in this article.

d) Imaging evaluation of tumor heterogeneity

Investigating tumor heterogeneity is a key point in cancer research. Tumors are highly heterogeneous on the histopathological level, with spatial variation in cellularity, angiogenesis, extracellular matrix, and necrosis. Moreover, heterogeneity in tumors already exists at the cell level and is highly influenced by the genetic background of tumor's cells as well as the environment where they develop [81].

Intra-tumor heterogeneity has implications on clinical outcome as well as on the development of adequate therapies, as it may limit an adequate diagnosis and is involved in tumor resistance to chemo- and radiotherapy. The identification of multiple cellular clones within tumors orientated newer therapies towards more personalized treatments; therefore, a better and more systematic appreciation of intra- and inter-tumor heterogeneity is crucial for drug development as well as for the accurate assessment of response to treatment. Thus, a better characterization of cancer biology with non-invasive methods in conjunction with an enhanced knowledge of the molecular, metabolic and genomic profile of tumors might help the development of new clinically relevant biomarkers.

It is difficult to assess tumor heterogeneity with invasive diagnostic methods as fine-needle aspiration or biopsy, as these do not represent the full extent of phenotypic or genetic variation within a tumor. On the contrary, imaging techniques, including MR imaging, CT and positron emission tomography (PET) are the ideal tools to analyze tumor heterogeneity in a non-invasive manner. The development of imaging techniques and dedicated software for quantitative and qualitative analysis have tremendously improved the evaluation of tumor heterogeneity over the last years. The strength of MR imaging compared with other imaging modalities resides in its potential to provide a vast array of different image contrasts, including T1, T2, contrast enhancement and perfusion, and DWI at a high spatial resolution and in a three-dimensional manner, providing unique insight into tumor heterogeneity.

Independently from the technique, there are several modalities for assessing tumor heterogeneity with cross-sectional imaging. Among them, histogram analysis is

more and more used. This methodology proved its usefulness for investigating the distributions of various parameters such as permeability in dynamic contrast-enhanced MR [82,83] and ADC in DW-MR imaging [84].

The histogram of an image is a function showing -for each intensity level- the number of pixels in the whole image having the same intensity. Histogram analysis uses descriptive parameters to report several quantitative factors, as mean, standard deviation, mode, maximum and minimum, kurtosis, skewness, and percentiles, entropy, etc. Mean and standard deviation represent average and dispersion of the histogram, respectively; kurtosis reflects the peakedness of the distribution and is a measure of the shape of the probability distribution; skewness is a measure of asymmetry of the probability distribution; entropy is a statistical measure of the irregularities in a histogram, allowing the description of the variation of a parameter of interest's distribution; finally, a percentile represents the value below which a percentage of observations is calculated. The meaning of these metrics in cancer studies is still under investigation; nevertheless, many studies agreed that histogram-derived parameters can be significant predictors of prognosis and response to treatment in various types of cancers. Most clinical studies using MR imaging histogram analysis were performed in the brain, but histogram analysis is increasingly used for extra-cranial oncologic imaging. Basing on previous reports, kurtosis, skewness and percentiles seem to be promising parameters for differentiating between different types of gliomas [85], between pseudo- and early progression in glioblastomas [86,87] and between cancer subtypes [88]. Percentiles, kurtosis and skewness of ADC distributions allowed grading of endometrial cancer [89]. Finally, histogram analysis of MR images showed its added value as predictor of response to treatment in various cancers [83,90-92].

Histogram analysis of ADC is particularly useful to evaluate tumor heterogeneity as it analyzes different microenvironments that may be masked by evaluating mean ADC values, as happens during the conventional analysis of DW images. Biomarkers estimated from DWI have been related to cancer aggressiveness and response to therapy. Nowadays, most studies report histogram investigations of ADC in tumors. For example, ADC histograms were found to be able to differentiate astrocytomas from oligodendrogliomas by statistical comparisons of

mean, mode, peak height, percentiles and skewness [94]; another study found that the 75th percentile ADC had the highest AUC (0.791) in differentiating intra-hepatica mass-forming cholangiocarcinoma from hepatocellular carcinoma, with sensitivity and specificity of 69.7% and 77.6%, respectively [94]. Differentiation of benign from malignant cervix tumors was possible by evaluating histograms of ADC distributions [84,95]: a significant difference was found between squamous cell carcinomas and adenocarcinomas in terms of skewness that supposedly reflects a more heterogeneous architecture of adenocarcinomas. The skewness and kurtosis of ADC histograms predicted response to angiogenic therapy in recurrent high-grade gliomas showing that patients with increased skewness had a shorter progression-free survival compared with patients with stable or decreased skewness [96]. Identification of early response in patients with newly diagnosed or recurrent ovarian cancer was possible demonstrating significantly decreased $ADC_{skewness}$ and $ADC_{kurtosis}$ after a third cycle of therapy [97]. Finally, metrics derived from ADC histograms have been also correlated to several immunohistochemical features of solid tumors. For example, Meyer et al [98] reported that the ADC_{max} correlated with p53 expression ($p = -0.446$, $p = 0.009$) and ADC_{mode} correlated with Her2-expression ($p = -0.354$, $p = 0.047$) in head and neck squamous cell carcinomas. Moreover, 25^{th} percentile, 90^{th} percentile and $ADC_{entropy}$ correlated with Hif1-alpha ($p = -0.423$, $p = 0.05$, $p = -0.494$, $p = 0.019$, $p = 0.479$, $p = 0.024$, respectively). $ADC_{kurtosis}$ correlated with P53 expression ($p = -0.466$, $p = 0.029$). Another study [99] revealed a strong correlation between EGFR expression and ADC_{max} ($p=0.72$, $P=0.02$), an inverse correlation between $ADC_{kurtosis}$ and $ADC_{skewness}$ with p53 expression ($p=-0.64$, $P=0.03$ and $p=-0.81$, $P=0.002$, respectively) and between ADC_{median} and ADC_{mode} with Ki67 ($p=-0.62$, $P=0.04$ and $p=-0.65$, $P=0.03$, respectively) in rectal cancer. Moreover, PD1-positive tumors showed statistically significant lower ADC_{max} values in comparison to PD1-negative tumors, 1.93 ± 0.36 vs $2.32 \pm 0.47 \times 10\text{-}3 mm2/s$, $p=0.04$.

2. Aims of the study

To evaluate MR-derived whole-tumor histogram analysis parameters in predicting aggressiveness of PDACs and neuroendocrine neoplasms panNENs, by correlating them to pathological features.

3. Materials and methods

a) Patient cohort

Between January 2013 and December 2017, 355 consecutive patients with PDAC or panNENs who underwent MR within 1 month before surgery at our institution were identified through a review of our pathologic and radiologic databases.

Inclusion criteria were: (a) optimal diagnostic quality MR images without any severe motion artifact; (b) unifocal disease; (c) patients who did not undergo local or systemic treatments before surgery, except for somatostatin analogues in hyperfunctioning panNENs; (d) patients who underwent demolitive surgery with standard or extended lymphadenectomy. Exclusion criteria were: (a) suboptimal diagnostic quality MR images with motion artifacts; (b) multifocal or diffuse disease with difficult delineation of tumor margins; (c) local or systemic treatments before surgery; (e) minimally invasive surgery without standard lymphadenectomy.

b) Pathological analysis

For every patient, an experienced pathologist (S.G., with 15 years of experience in pancreatic diseases) reviewed the histological reports and the resection specimens and recorded the following features: tumor size; grade, according to the 2010 WHO classification [20]; absence (-) or the presence (+) of vascular infiltration (V), nodal metastases (N) and liver metastases (M). Vascular infiltration was assessed during surgery. Final diagnosis of liver metastases was obtained with percutaneous US-guided FNA or at pathological analysis of resection specimens.

c) MR Imaging: technical parameters and examination protocol

All examinations were performed with a 1.5 T unit (Aera, Siemens Medical Solutions, Erlangen, Germany) with a multi-channel phased-array torso coil. Baseline MR sequences included breath-hold axial, coronal, sagittal and para-coronal T2-weighted (T2w) imaging with a half-Fourier acquisition single-shot turbo spin-echo (HASTE) sequence, axial T2w fat-suppressed (FS) sequence, axial T1-weighted (T1w) Dixon sequence; diffusion-weighted imaging using a free-breathing single-shot echo-planar imaging pulse sequence with b values of 50, 400,

and 800 sec/mm2, with automatic reconstruction of ADC maps; and a breath-hold T1w FS gradient-echo sequence (volume-interpolated breath-hold examination, VIBE). Dynamic MR images were obtained by using the FS three-dimensional gradient-echo sequence before and after administration of gadopentate dimeglumine (Multihance; Bracco, Milan, Italy) at a dose of 0.1 mmol per kilogram of body weight at an injection rate of 2 mL/sec. The timing for post-contrast imaging was determined by fixed delays (30-45 seconds after the start of contrast medium administration for arterial phase imaging; 60-70 seconds
for portal phase imaging; and >180 seconds for delayed phase imaging). The acquisition of three-dimensional gradient-echo data for each phase was acquired during breath hold at end expiration. Detailed MR imaging parameters are summarized in table 1.

Table 1 MR imaging acquisition protocol

Sequence and imaging plane	**TR/TE (msec)**	**Field of View (mm)**	**Matrix**	**Flip Angle (degrees)**	**Thickness (mm)**
T2w					
Axial	∞/90	400-450	512x384	180	6
Coronal	∞/90	400-450	364x384	180	6
Sagittal	∞/90	390-400	253x512	180	4
Paracoronal	∞/90	400-430	253x512	180	4
DW axial	6000/59	400-440	192x144	90	6-6.5
T2w FS axial	2900/82	400-460	384x174	160	6-6.5
T1w chemical-shift axial	6.69/2.39-4.77	400-430	320x173	10	3-3.5
T1w FS					
Axial	6.1/2.4	400-480	320x256	10	3-3.5
Coronal	6.1/2.4	400-450	187x256	10	3
2D MRCP	∞/746	300	384x384	180	70

Legend: *TR*, repetition time; *TE*, time of echo; *T2w*, T2-weighted; *DW*, diffusion-weighted; *FS*, fat suppressed; *T1w*, T1-weighted; *MRCP*, magnetic resonance cholangiopancreatography.

d) Image analysis

All MR data were digitally transferred from a picture archiving and communication system workstation to a personal computer. Image analysis was performed by two radiologists in consensus (R.D. and N.C., with 10 and 8 years of experience in abdominal MR imaging) who were blinded to the pathologic results by using a software for medical image processing (MevisLab; Mevis Medical Solutions, Bremen, Germany) loaded with an in-house graphical user interface. The axial MR sequence in whom the tumor showed its highest conspicuity was chosen for tumor segmentation; ROIs were manually drawn in every contiguous slice containing the tumor and then copied onto the other MR sequences. Tumor boundaries were defined by correlating all MR images, including high b-value DW images. The data acquired from each slice were then automatically summated to derive volumes of interest (VOIs). Each tumor segmentation took a median of 8 minutes (range, 5-20 minutes). Histograms were obtained from axial Dixon-derived in phase T1w, T1w FS, T2w, T2w FS, and postcontrast images, as well as the ADC maps. Histogram analysis of the distribution of intensity and ADC values was performed by using mathematical analytical software (Matlab 2009a; Mathworks, Natick, USA). Several quantitative parameters were derived: skewness, mean, kurtosis, variance, entropy, standard deviation (SD), minimum, maximum, median, 25th percentile, 75th percentile, 95th percentile, interquartile range (IQR) and uniformity. As previously reported by Sidhu et al [100], absolute T2 and T1 weighted signal intensities are not comparable across patients without standardization, unlike ADC maps; therefore, T1 and T2 mean, variance, SD, minimum, maximum, median, percentiles and IQR were not analyzed further.

e) Statistical analysis

All statistical analyses were performed with commercially available software (SPSS 23; SPSS, Chicago, USA; and MedCalc 17.9; MedCalc Software, Mariakerke, Belgium). For the purpose of statistical analysis, basing on their similar biological behavior [30,101], well- and moderately differentiated PDACs as well as G2 and G3 panNENs were grouped and considered together.

Histogram-derived parameters were then compared among pathological features of the tumors (i.e., low vs high grade; V- vs V+; N- vs N+; and M- vs M+) using Mann-Whitney U test.

Receiver operating characteristic (ROC) curves were constructed to determine the optimum threshold for each histogram parameter to identify poorly differentiate/G2-3, V+, N+ and M+ tumors, and optimal cutoff points were individuated according to the Youden's index, with calculation of sensitivity and specificity. Pairwise comparison of ROC curves was performed by calculating the standard error of the area under the curve (AUC) and the difference between the AUCs, according to the method described by Delong et al [102].

For all statistical analyses, a p value less than .05 was considered to indicate a significance difference.

4. Results

a) Study population

One hundred-eighty-six patients were excluded from this study for the following reasons: suboptimal image quality of MR examinations, with severe motion artifacts from limited breath holding (n= 125); enucleation of a tumor smaller than 1 cm (n= 11; all insulinomas); and previous therapy (n= 50). Finally, 169 patients (mean age, 60.5 years; age range, 24-81 years) were included in this study. There were 127 PDACs (mean age, 66.2 years; age range, 45-81 years) and 42 panNENs (mean age, 54.9 years; age range, 24-75 years).

b) Pathological analysis

All primary tumors were successfully resected (127 pancreaticoduodenectomies; 40 distal pancreatectomies; 2 total pancreatectomies). Details are presented in table 2.

Table 2 Clinicopathological data of the study population

Feature	PDACs	panNENs	Total
Number of cases	127 (75.1%)	42 (24.9%)	169 (100%)
Age (mean, range)	66.2 (45-81)	54.9 (24-75)	60.5 (24-81)
Sex			
Male	77 (60.6%)	23 (54.8%)	100 (59.2%)
Female	50 (39.4%)	19 (45.2%)	69 (40.8%)
Grade			
WD/G1	2 (1.6%)	18 (42.8%)	20 (11.8%)
MD/G2	114 (89.8%)	21 (50%)	135 (79.9%)
PD/G3	11 (8.6%)	3 (7.2%)	14 (8.3%)
Location			
Head	109 (85.8%)	18 (42.9%)	127 (75.1%)
Body	15 (11.8%)	15 (35.7%)	30 (%)
Tail	3 (2.4%)	9 (21.4%)	12 (%)
Surgery			
PaD	109 (85.8%)	18 (42.9%)	127 (75.1%)
DP	16 (12.6%)	24 (57.1%)	40 (23.7%)
TP	2 (1.6%)	0 (0%)	2 (1.2%)
Vascular infiltration			
No	99 (77.9%)	35 (83.3%)	134 (79.3%)
Yes	28 (22.1%)	7 (16.7%)	35 (20.7%)
Nodal metastases			
No	25 (19.7%)	19 (45.2%)	44 (26%)
Yes	102 (80.3%)	23 (54.8%)	125 (74%)
Liver metastases			
No	127 (100%)	35 (83.3%)	162 (95.9%)
Yes	0 (0%)	7 (16.7%)	7 (4.1%)

Data are expressed as number of cases (%), unless otherwise indicated. Legend: *WD*, well differentiated; *MD*, moderately differentiated; *PD*, poorly differentiated; *PaD*, pancreaticoduodenectomy; *DP*, distal pancreatectomy; *TP*, total pancreatectomy.

PDACs

At pathological analysis there were 2 well differentiated (WD) PDACs (1.6%), 114 moderately differentiated (MD) PDACs (89.8%) and 11 poorly differentiated (PD) PDACs (8.6%). Most PDACs were located in the pancreatic head (N=109, 85.8%), 15 were located in the pancreatic body (11.8%) and 3 (2.4%) in the pancreatic tail. Vascular involvement was identified at pre-operative MR in 28 cases (22.1%) and confirmed during surgery in all cases. Nodal metastases were diagnosed in 102 cases (80.3%). None of the patients with PDAC had liver metastases. Mean size of PDACs was 27.8 mm (7-60 mm).

panNENs

Regarding panNENs, there were 18 G1 tumors (42.8%), 21 G2 tumors (50%) and 3 G3 tumors (7.2%). All panNENs had well differentiated morphology at pathological analysis. Eighteen panNENs were located in the pancreatic head (42.9%), 15 were located in the pancreatic body (35.7%) and 9 (21.4%) in the pancreatic tail. Vascular involvement was identified at pre-operative MR in 7 cases (16.7%) and confirmed during surgery in all cases. Nodal metastases were diagnosed in 19 cases (45.2%). Seven patients with panNEN had liver metastases (16.7%); all patients with liver metastases were correctly identified by MR. The pathological confirmation of liver metastases was obtained after surgical resection in 4 cases and with pre-operative FNA in 3 cases. Mean size of panNENs was 32.6 mm (11-105 mm).

c) Histogram analysis

The results of the Mann-Whitney's U test for the comparison between histogram-derived parameters and pathological features are presented in tables 3-8.

Table 3 Comparison between histogram-derived parameters and presence of vascular involvement in PDACs.

Vascular involvement	**$T2fs_{entropy}$**	**$T2_{entropy}$**	**$ADC_{entropy}$**
V-[a]	6.67 ± 0.7	7.47 ± 0.64	6.88 ± 0.89
V+ [a]	7.03 ± 0.61	7.58 ± 0.39	7.46 ± 0.89
P	.044	.048	.022
AUC	.626	.623	.641

[a]Data are mean ± standard deviation.

Table 4 Comparison between histogram-derived parameters and presence of nodal metastases in PDACs.

Nodal metastases	**$ADC_{skewness}$**
N-[a]	0.21 ± 0.57
N+[a]	0.54 ± 0.69
P	.027
AUC	.642

[a]Data are mean ± standard deviation.

PDACs

No significant differences were among histogram-derived parameters of PDACs of different grade. The results of ROC analysis for significantly different histogram-derived parameters in PDACs are presented in tables 3 and 4.

$T2_{entropy}$, $T2fs_{entropy}$, and $ADC_{entropy}$ were significantly higher in V+ PDACs compared with V- tumors. At ROC analysis, there were no significant differences between the AUCs of $T2_{entropy}$, $T2fs_{entropy}$ and $ADC_{entropy}$ for the identification of PDACs with vascular infiltration (figures 1 and 2), even though $ADC_{entropy}$ reported the highest AUC (.641); at a cut-off of 6.65, this parameter identified V+ PDACs with 92.9% specificity and 35.3% specificity.

$ADC_{skewness}$ was significantly higher in N+ PDACs compared with N- tumors (AUC=.642; figure 3). At a given cut-off value of 0.52, $ADC_{skewness}$ identified N+ PDACs with 53.9% sensitivity and 72% specificity.

No significant differences between groups were found for other histogram-derived parameters ($p > .05$).

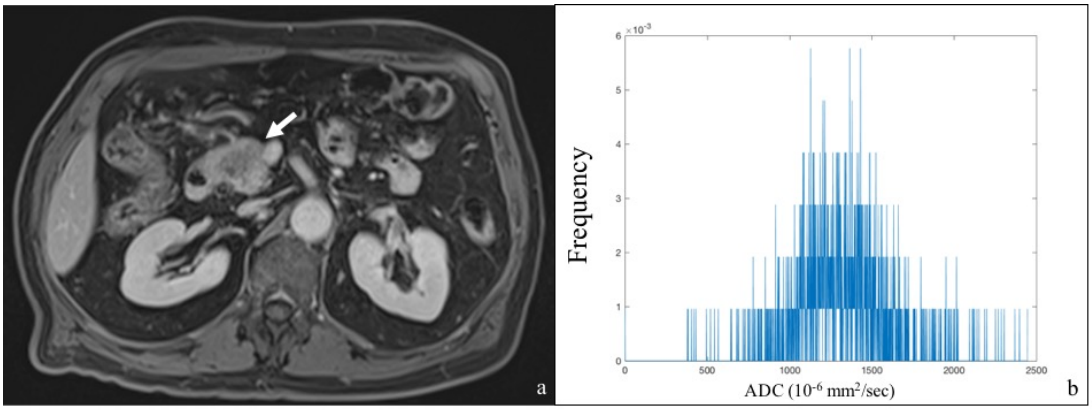

Figure 1. Findings in a 62-year-old man with a ductal adenocarcinoma of the pancreatic head. (a) On axial portal phase T1-weighted image the tumor is homogeneously hypointense; infiltration of the superior mesenteric vein can be seen (arrow). (d) Whole-tumor histogram analysis of ADC values provided high entropy value (7.50).

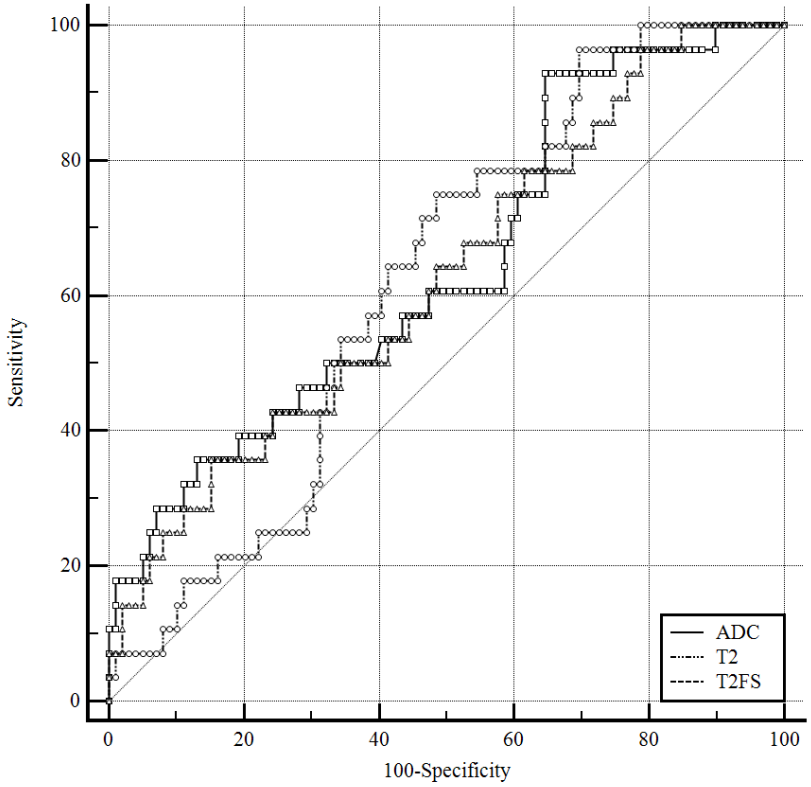

Figure 2. Comparison of ROC curves of $ADC_{entropy}$, $T2_{entropy}$ and $T2fs_{entropy}$ for the identification of V+ PDACs.

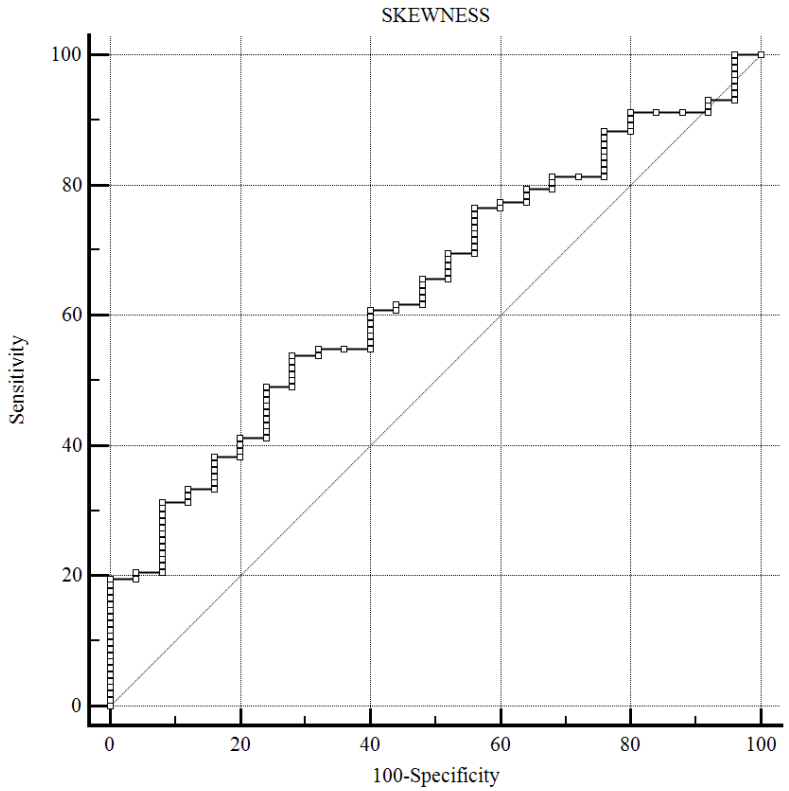

Figure 3. ROC curve of $ADC_{skewness}$ for identification of N+ PDACs.

PanNENs

$T2_{skewness}$, $ADC_{kurtosis}$, and $ADC_{entropy}$ were significantly higher in G2-3 tumors compared with G1 tumors, as well as in V+ compared with V- tumors; $ADC_{uniformity}$ was significantly lower in G2-3 tumors compared with G1 tumors and in V+ compared with V- panNENs (figures 4 and 5).

$ADC_{kurtosis}$ and $ADC_{entropy}$ were significantly higher in N+ panNENs compared with N- tumors; ADC_{median} and ADC_{75} were significantly lower in N+ compared with N- panNENs. Finally, $ADC_{kurtosis}$ and ADC_{max} were significantly higher in M+ compared with M- tumors (figure 6). No significant differences between groups were found for other histogram-derived parameters ($p > .05$).

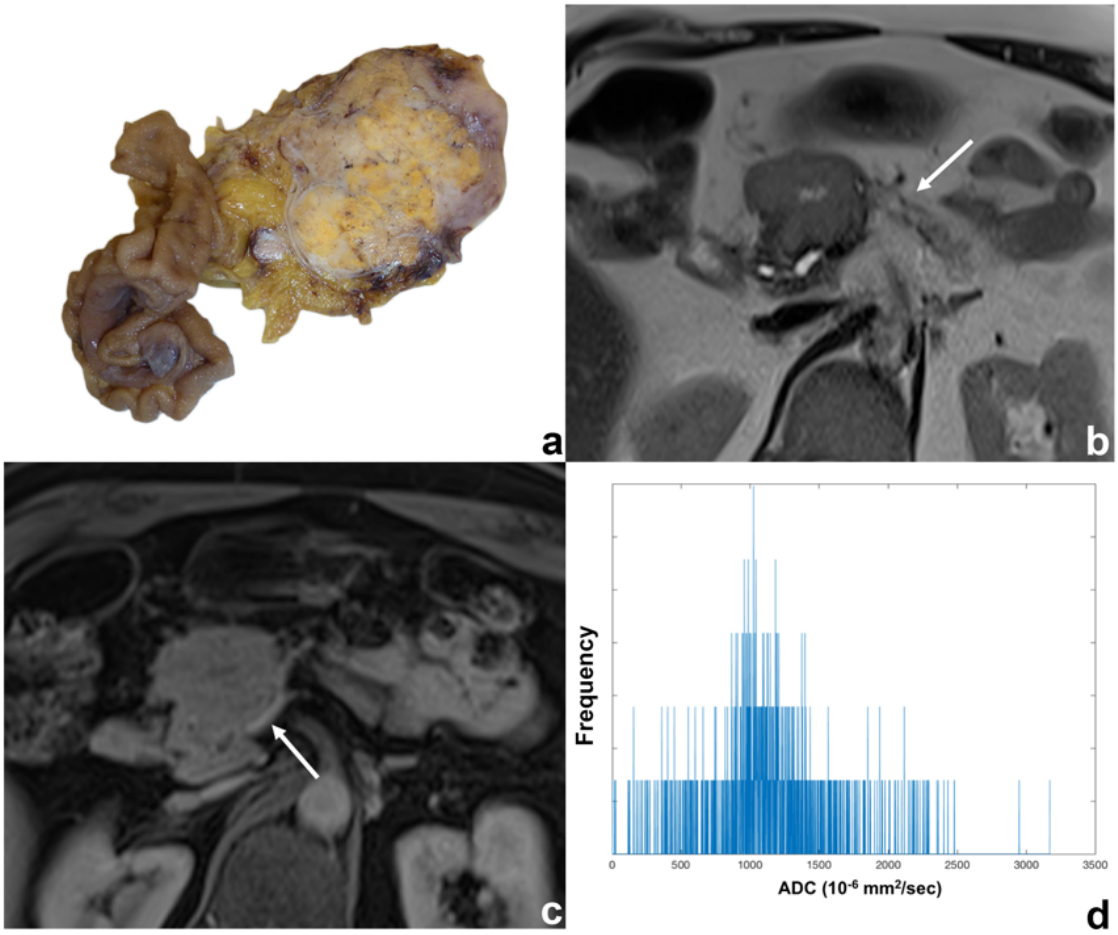

Figure 4 (a-d). Findings in a 54-year-old man with a G2 neuroendocrine tumor of the pancreatic head. (a) Resection specimen (pancreaticoduodenectomy; transverse cut): at histopathologic examination the tumor shown to a be a G2 (Ki67=5%), N1 panNEN. (b) On axial T2-weighted image the tumor is inhomogeneously hyperintense; upstream chronic obstructive pancreatitis can be seen (arrow). (c) Infiltration of the superior mesenteric vein can be seen on postcontrast portal phase image (arrow). (d) Whole-tumor histogram analysis of ADC values provided high entropy and kurtosis values (9.01 and 4.68).

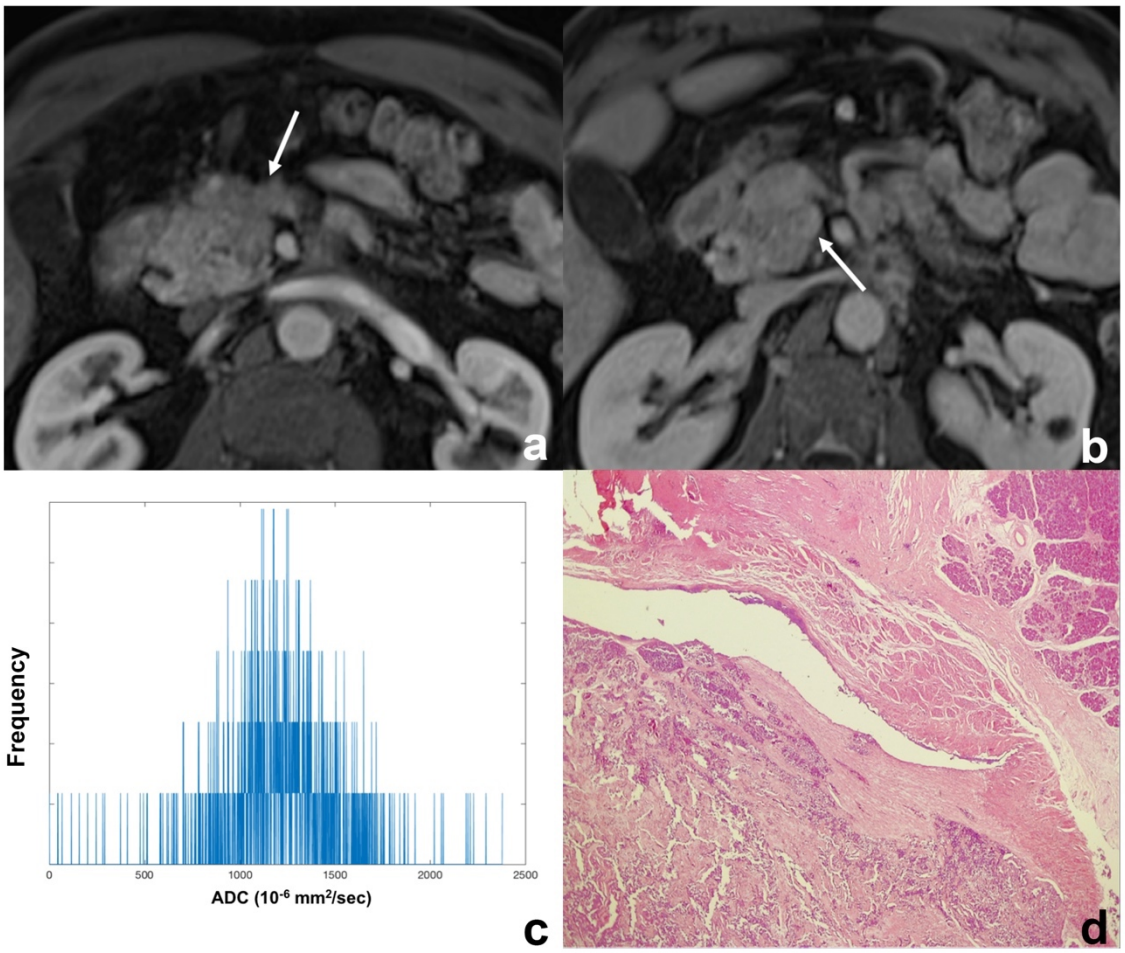

Figure 5 (a-d). Findings in a 55-year-old man with a pancreatic head neuroendocrine tumor associated with vascular infiltration. (a) On postcontrast arterial phase MR image the tumor is hypointense and present ill-defined margins (arrow). (b) Infiltration of the superior mesenteric vein can be seen on postcontrast portal phase image (arrow). (c) Histogram of whole-lesion ADC values shows a sharp peak, consistent with high kurtosis (5.56); entropy was 8.91. (d) Histopathologic examination shown that the tumor was a G2 (Ki67=15%), N1 and confirmed tumor infiltration of the superior mesenteric vein (Hematoxylin-eosin stain; original magnification, ×100).

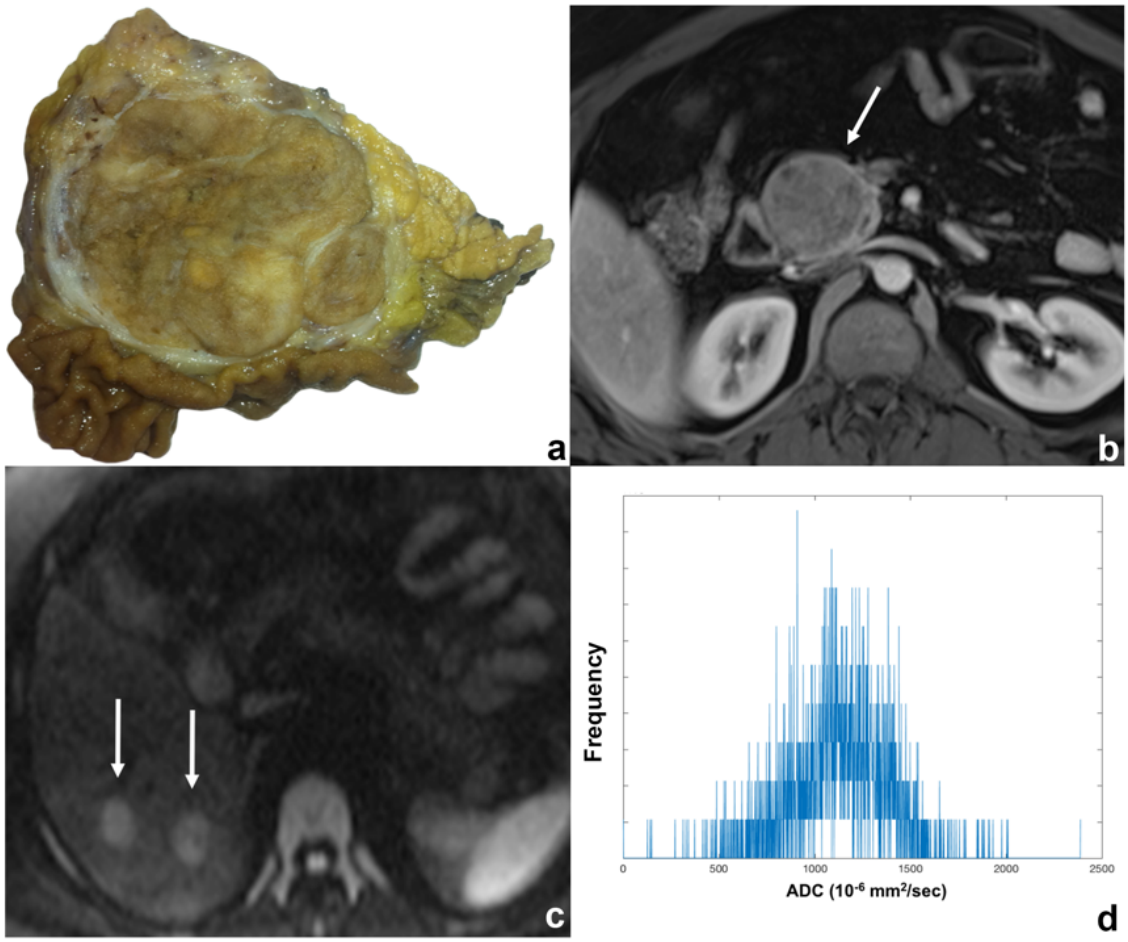

Figure 6 (a-d). Findings in a 47-year-old man with a pancreatic head neuroendocrine tumor associated with liver metastases. (a) Resection specimen (pancreaticoduodenectomy; transverse cut); the tumor shown to be a G2 (Ki67=5%), N1 panNEN. (b) On postcontrast arterial phase MR image the tumor shows inhomogeneous enhancement (arrow). (c) Liver metastases can be seen on DW image (arrows). (d) Histogram of whole-lesion ADC values demonstrated a sharp peak, indicating high kurtosis (4.01); entropy was 9.44.

The results of ROC analysis for significantly different histogram-derived parameters are presented in tables 5-8. At ROC analysis, $ADC_{entropy}$ had the highest AUC for the identification of G2-3 tumors (.757); sensitivity and specificity for the identification of G2-3 panNENs were 83.3% (95% CI: 61.2-94.5) and 61.1% (95% CI: 36.1-81.7). $ADC_{kurtosis}$ showed the highest AUC under the ROC curve for identifying V+, N+ and M+ panNENs (.820, .709, and .820, respectively; figures 5, 6 and 7); sensitivity and specificity were: 85.7/74.3% (95% CI: 42-99.2 /56.4-86.9); 36.8/96.5% (95% CI: 17.2-61.4 /76-99.8); and 100/62.8% (95% CI: 56.1-100/44.9-78.1).

Pairwise comparison did not show any significant difference between ROC curves (figure 7).

Table 5 Comparison between histogram-derived parameters and tumor grade in panNENs.

Grade	**$T2_{skewness}$**	**$ADC_{kurtosis}$**	**$ADC_{entropy}$**	**$ADC_{uniformity}$**
G1[a]	0.37 ± 0.78	2.95 ± 1.35	5.95 ± 2.34	0.015 ± 0.015
G2-3[a]	0.9 ± 0.85	5.95 ± 7.95	7.95 ± 1.55	0.006 ± 0.008
P	.040	.015	.005	.014
AUC	.688	.720	.757	.722

[a]Data are mean ± standard deviation.

Table 6 Comparison between histogram-derived parameters and presence of vascular involvement in panNENs.

Vascular involvement	**$T2_{skewness}$**	**$ADC_{kurtosis}$**	**$ADC_{entropy}$**	**$ADC_{uniformity}$**
V-[a]	1.37 ± 1.06	3.54 ± 2.37	6.77 ± 2.18	0.011 ± 0.013
V+ [a]	0.54 ± 0.75	5.58 ± 2.95	8.70 ± 1.02	0.003 ± 0.002
P	.045	.008	.028	.041
AUC	.688	.820	.763	.747

[a]Data are mean ± standard deviation.

Table 7 Comparison between histogram-derived parameters and presence of nodal metastases in panNENs.

Nodal metastases	**$ADC_{kurtosis}$**	**$ADC_{entropy}$**	**ADC_{median}**	**ADC_{75}**
N-[a]	3.08 ± 1.22	6.31 ± 2.38	1273.5 ± 345.91	1552.81 ± 452.18
N+[a]	4.84 ± 3.36	8.04 ± 1.35	1079.45 ± 217.40	1302.59 ± 218.31
P	.021	.027	.042	0.24
AUC	.709	.700	.684	.705

[a]Data are mean ± standard deviation.

Table 8 Comparison between histogram-derived parameters and presence of liver metastases.

Liver metastases	**$ADC_{kurtosis}$**	**ADC_{max}**
M-[a]	3.26 ± 1.27	2235.63 ± 622.5
M+ [a]	6.94 ± 4.75	2832.71 ± 533.01
P	.008	.019
AUC	.820	.784

[a]Data are mean ± standard deviation.

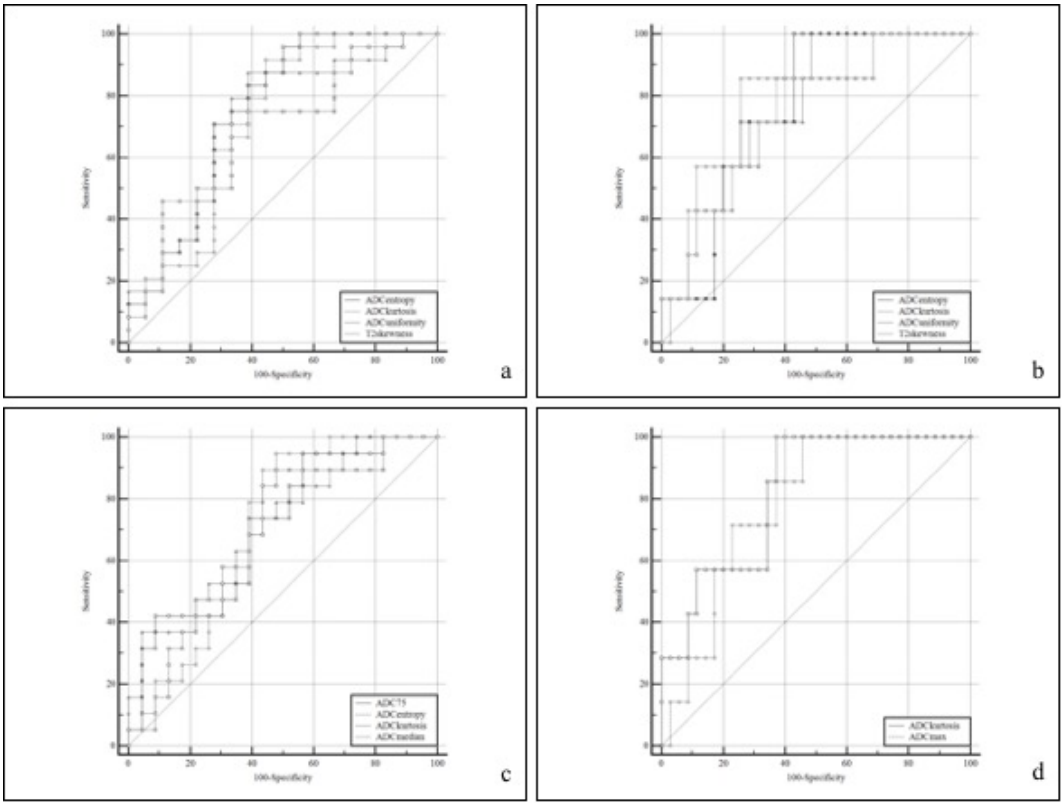

Figure 7. Comparison of histogram-derived ROC curves. (a) ROC curves of ADC entropy, kurtosis, uniformity and $T2_{skewness}$ for the identification of G2-3 panNENs. (b) ROC curves of ADC entropy, kurtosis, uniformity and T2skewness for the identification of V+ panNENs. (c) ROC curves of ADC entropy, kurtosis, median and 75th percentile for the identification of N+ panNENs. (d) ROC curves of ADC kurtosis and maximum value for the identification of M+ tumors.

5. Discussion

This study evaluated the diagnostic accuracy of histogram-derived MR parameters in predicting grade and aggressiveness in PDACs and panNENs. Previous work [103] suggested that histogram analysis of ADC maps can be useful in differentiating histologic grades of panNENs. Our results confirm these findings: in the present study, $ADC_{entropy}$ was the parameter with the highest accuracy in identifying high grade panNENs (AUC=.757), with 83.3% sensitivity. $ADC_{entropy}$ was also the parameter with the highest accuracy in identifying PDACs with vascular infiltration (AUC=.641, specificity 92.2%). $ADC_{kurtosis}$ was found to be the parameter with the highest diagnostic accuracy (AUC= .820, .709, and .820, respectively) for the identification of panNENs with vascular infiltration, nodal and hepatic metastases: sensitivity and specificity of this parameter were 85.7/74.3%, 36.8/96.5%, and 100/62.8%, respectively. Finally, $ADC_{skewness}$ was significantly higher in PDACs with nodal metastases compared with N- tumors (p=.027; AUC=.642), with a reported specificity of 72%.

Histogram analysis of ADC data can interrogate the biologic heterogeneity of tumors by classifying domains of different diffusivity, which may have prognostic and predictive implications [74]. Two quantities calculated by using this histogram analysis are uniformity and entropy. These parameters characterize the uniformity and the irregularity of intra-tumor voxel distribution [104,105]. When histogram analysis is performed on solid tumors, entropy and uniformity therefore reflect and quantify intratumoral heterogeneity. Kurtosis is a measure of the magnitude of pixel distribution, representing how peaked a histogram is; on the ADC histogram distribution, kurtosis represents the position of peak height that indicate the ADC value of the maximum frequency [85]. Such metrics demonstrated to be reliable markers of tumor heterogeneity, with correlation to the structural, physiological, molecular and metabolic changes occurring upon tumor progression and during therapy [85]. Higher kurtosis and entropy, as well as lower uniformity, are thought to represent microstructural and functional heterogeneity and are associated with poorer prognosis [85]. Our results confirm this hypothesis, as both $ADC_{entropy}$ and $ADC_{kurtosis}$ were significantly higher in panNENs with higher malignancy compared

to G1, V-, N- and M- tumors (all p <.05); $ADC_{entropy}$ was also significantly higher in PDACs infiltrating peri-pancreatic vessels compared to V- tumors.

Skewness is another metric of heterogeneity, representing a measure of asymmetry of the probability distribution. In the present study, $ADC_{skewness}$ was found to be only significant predictor of nodal metastases in PDACs: N+ PDACs had significantly higher $ADC_{skewness}$ compared to N- PDACs.

There are very few studies on MR histogram analysis of pancreatic tumors.

ADC histograms may be helpful in differentiating between pancreatic cancer and focal pancreatitis as well as between PDACs and panNENs. Ma et al [106] found that 50^{th} and 100^{th} ADC percentiles can reflect tissue heterogeneity and help differentiate normal pancreas from focal pancreatitis and PDAC. Shindo et al [107] reported that ADC histogram analysis can help differentiate PDACs from panNENs: the mean ADC200 and ADC400 were significantly higher in panNENs than in PDACs (P=0.001 and P=0.019, respectively); PDACs showed significantly higher skewness and kurtosis on ADC400 (P=0.007 and P=0.001, respectively) and ADC800 (P=0.001 and P=0.001, respectively). With all b-value combinations, the entropy of ADC values was significantly higher in PDACs (P<0.001 for ADC200; P=0.001 for ADC400; P<0.001 for ADC800), and showed the highest area under the ROC curve for diagnosing carcinomas (0.77 for ADC200, 0.76 for ADC400, and 0.78 for ADC800).

Histogram-derived parameters may also be helpful in identifying pancreatic tumors with higher malignant potential. Pereira et al [103] found that histographic analysis of ADC maps on the basis of the entire tumor volume can be useful in differentiating histologic grades of panNENs: the mean, 75th, 90th, and 95^{th} percentiles were significantly higher in G1 tumors compared to G2 and to G3 tumors; ADC skewness and kurtosis were significantly different between G1 and G3 tumors. Hoffman et al [108] reported that $ADC_{entropy}$ may serve as a biomarker for identifying the malignant potential of intraductal papillary mucinous neoplasms (IPMNs). In this study, ADC histogram metrics demonstrating significant differences between benign and malignant IPMNs were: entropy (5.1 ± 0.2 vs. 5.4 ± 0.2; p = 0.01, AUC = 86%); mean of the bottom 10th percentile (2.2 ± 0.4 vs. 1.6 ± 0.7; p = 0.03; AUC = 81%); and mean of the 10-25th percentile (2.8 ± 0.4 vs. 2.3

± 0.6; p = 0.04; AUC = 79%). For $ADC_{entropy}$, an optimal threshold of >5.3 achieved a sensitivity of 100%, a specificity of 70%, and an accuracy of 83% for predicting malignancy in pancreatic IPMNs.

Considering our results and the aforementioned studies, imaging of tumor heterogeneity may provide a non-invasive assessment of aggressiveness and prognosis in pancreatic tumors.

The retrospective nature of this study was a limitation. Other limitations are the small amount of WD and PD PDACs and G3 panNENs as well as the small number of panNENs with vascular infiltration and liver metastases. Moreover,

the inclusion criteria of this study may have been resulted in a selection bias, as unresectable PDACs were excluded; histogram-derived distributions in this group of tumors remains to be evaluated.

6. Conclusions

Whole-tumors histogram analysis of ADC values may represent a valuable non-invasive tool in predicting the aggressiveness of PDACs and panNENs. Our results indicate that histogram metrics related to intra-tumor heterogeneity, as $ADC_{entropy}$, $ADC_{kurtosis}$ and $ADC_{skewness}$ are the most accurate parameters for the identification of PDACs and panNENs with higher biological aggressiveness. Further and larger studies are needed to incorporate the results of the histogram analysis within decision support models and to mine these data to detect possible correlations with genomic patterns.

7. References

1. Malvezzi M, Bertuccio P, Levi F, La Vecchia C, Negri E. European cancer mortality predictions for the year 2014. Ann Oncol. 2014;25:1650–1656.
2. Yeo TP. Demographics, epidemiology, and inheritance of pancreatic ductal adenocarcinoma. Semin Oncol. 2015;42:8–18.
3. Larsson SC, Wolk A. Red and processed meat consumption and risk of pancreatic cancer: meta-analysis of prospective studies. Br J Cancer. 2012;106:603–607.
4. Ojajarvi IA, Partanen TJ, Ahlbom A, et al. Occupational exposures and pancreatic cancer: a meta-analysis. Occup Environ Med. 2000; 57:316–324.
5. Ducreux M, Cuhna AS, Caramella C, et al. Cancer of the pancreas: ESMO Clinical Practice Guidelines for diagnosis, treatment and follow-up. Ann Oncol. 2015;26: v56–v68.
6. Hammel P, Huguet F, van Laethem JL, et al. Effect of Chemoradiotherapy vs Chemotherapy on Survival in Patients With Locally Advanced Pancreatic Cancer Controlled After 4 Months of Gemcitabine With or Without Erlotinib: The LAP07 Randomized Clinical Trial. JAMA. 2016;315(17):1844-1853.
7. Shinchi H, Takao S, Noma H, et al. Length and quality of survival after external-beam radiotherapy with concurrent continuous 5-fluorouracil infusion for locally unresectable pancreatic cancer. Int J Radiat Oncol Biol Phys. 2002;53:146–150.
8. Sultana A, Tudur Smith C, Cunningham D, et al. Systematic review, including meta-analyses, on the management of locally advanced pancreatic cancer using radiation/combined modality therapy. Br J Cancer. 2007; 96:1183–1190.
9. Chauffert B, Mornex F, Bonnetain F, et al. Phase III trial comparing intensive induction chemoradiotherapy (60 Gy, infusional 5-FU and intermittent cisplatin) followed by maintenance gemcitabine with gemcitabine alone for locally advanced unresectable pancreatic cancer.

Definitive results of the 2000-01 FFCD/SFRO study. Ann Oncol. 2008;19(9):1592-1599.

10. Loehrer PJ Sr, Feng Y, Cardenes H, et al. Gemcitabine alone versus gemcitabine plus radiotherapy in patients with locally advanced pancreatic cancer: an Eastern Cooperative Oncology Group trial. J Clin Oncol. 2011;29:4105–4112.
11. Mukherjee S, Hurt CN, Bridgewater J, et al. Gemcitabine-based or capecitabine- based chemoradiotherapy for locally advanced pancreatic cancer (SCALOP): a multicentre, randomised, phase 2 trial. Lancet Oncol. 2013;14:317–326.
12. NCCN guidelines for Pancreatic Adenocarcinoma, v. 2.2018.
13. Von Hoff DD, Ervin T, Arena FP, et al. Increased survival in pancreatic cancer with nab-paclitaxel plus gemcitabine. N Engl J Med. 2013;369(18):1691-1703.
14. Conroy T, Desseigne F, Ychou M, et al. FOLFIRINOX versus gemcitabine for metastatic pancreatic cancer. N Engl J Med. 2011;364(19):1817-1825.
15. Rishi A, Goggins M, Wood LD, Hruban RH. Pathological and molecular evaluation of pancreatic neoplasms. Semin Oncol. 2015;42:28–39.
16. Wisnoski NC, Townsend CM Jr, Nealon WH, Freeman JL, Riall TS. 672 patients with acinar cell carcinoma of the pancreas: a population-based comparison to pancreatic adenocarcinoma. Surgery. 2008;144:141–148.
17. Esposito I, Konukiewitz B, Schlitter AM, Klöppel G. Pathology of pancreatic ductal adenocarcinoma: facts, challenges and future developments. World J Gastroenterol. 2014; 20:13833–13841.
18. Yachida S, Iacobuzio-Donahue CA. Evolution and dynamics of pancreatic cancer progression. Oncogene. 2013;32(45):5253-5260.
19. Waddell N, Pajic M, Patch AM, et al. Whole genomes redefine the mutational landscape of pancreatic cancer. Nature. 2015;518:495–501.
20. Bosman FT, Carneiro F, Hruban RH, Theise N, editors. WHO Classification of Tumors of the Digestive System. Lyon: IARC Press; 2010. pp. 13–14.

21. Milione M, Maisonneuve P, Spada F et al. The clinicopathologic heterogeneity of grade 3 gastroenteropancreatic neuroendocrine neoplasms: Morphological differentiation and proliferation identify different prognostic categories. Neuroendocrinology 2017;104:85–93.
22. Cives M, Strosberg JR. Gastroenteropancreatic neuroendocrine tumors. CA Cancer J Clin. 2018 Oct 8 [Epub ahead of print].
23. Service FJ, McMahon MM, O'Brien PC, Ballard DJ. Functioning insulinoma - incidence, recurrence, and long-term survival of patients: a 60-year study. Mayo Clin Proc. 1991;66:711-719.
24. Whipple AO. Islet cell tumours of pancreas. Can Med Assoc J. 1952;66:334-342.
25. Jensen RT. Gastrinomas: advances in diagnosis and management. Neuroendocrinology. 2004;80:23-27.
26. Verner JV, Morrison AB. Islet cell tumor and a syndrome of refractory watery diarrhea and hypokalemia. Am J Med. 1958;25:374-380.
27. van Beek AP, de Haas ER, van Vloten WA, Lips CJ, Roijers JF, Canninga-van Dijk MR. The glucagonoma syndrome and necrolytic migratory erythema: a clinical review. Eur J Endocrinol. 2004;151:531-537.
28. Oberg K. Management of functional neuroendocrine tumors of the pancreas. Gland Surg. 2018;7:20-27.
29. Falconi M, Eriksson B, Kaltsas G, et al. ENETS Consensus Guidelines Update for the Management of Patients with Functional Pancreatic Neuroendocrine Tumors and Non-Functional Pancreatic Neuroendocrine Tumors. Neuroendocrinology 2016;103(2):153-171.
30. Halfdanarson TR, Rabe KG, Rubin J, Petersen GM. Pancreatic neuroendocrine tumors (PNETs): incidence, prognosis and recent trend toward improved survival. Ann Oncol. 2008;19:1727-1733.
31. Gorelik M, Ahmad M, Grossman D, Grossman M, Cooperman AM. Nonfunctioning incidental pancreatic neuroendocrine tumors: who, when, and how to treat? *Surg Clin North Am.* 2018;98:157-167.

32. Yao JC, Hassan M, Phan A, et al. One hundred years after ‘carcinoid’: epidemiology of and prognostic factors for neuroendocrine tumors in 35,825 cases in the United States. J Clin Oncol. 2008;26:3063–3072.
33. Cheslyn-Curtis S, Sitaram V, Williamson RC. Management of non-functioning neuroendocrine tumours of the pancreas. Br J Surg 1993;80:625–627.
34. Madura JA, Cummings OW, Wiebke EA, et al: Nonfunctioning islet cell tumors of the pancreas: a difficult diagnosis but one worth the effort. Am Surg 1997;63:573–577.
35. Matthews BD, Heniford BT, Reardon PR, et al: Surgical experience with nonfunctioning neuroendocrine tumors of the pancreas. Am Surg 2000; 66: 1116–1122.
36. White TJ, Edney JA, Thompson JS, et al: Is there a prognostic difference between functional and nonfunctional islet cell tumors? Am J Surg 1994; 168: 627–629.
37. Chu QD, Hill HC, Douglass HO Jr, et al: Predictive factors associated with long-term survival in patients with neuroendocrine tumors of the pancreas. Ann Surg Oncol 2002; 9:855–862.
38. Schurr PG, Strate T, Rese K, et al: Aggressive surgery improves long-term survival in neuroendocrine pancreatic tumors: an institutional experience. Ann Surg 2007;245:273– 281.
39. Bilimoria KY, Talamonti MS, Tomlinson JS, et al: Prognostic score predicting survival after resection of pancreatic neuroendocrine tumors: analysis of 3,851 patients. Ann Surg 2008;247:490–500.
40. Bettini R, Boninsegna L, Mantovani W, et al: Prognostic factors at diagnosis and value of WHO classification in a mono-institutional series of 180 non-functioning pancreatic endocrine tumours. Ann Oncol 2008;19:903– 908.
41. Scarpa A, Mantovani W, Capelli P, et al: Pancreatic endocrine tumors: improved TNM staging and histopathological grading permit a clinically efficient prognostic stratification of patients. Mod Pathol 2010;23:824–833.

42. Triponez F, Dosseh D, Goudet P, et al: Epidemiology data on 108 MEN-1 patients from the GTE with isolated nonfunctioning tumors of the pancreas. Ann Surg 2006;243: 265–272.
43. Hammel PR, Vilgrain V, Terris B, et al: Pancreatic involvement in von Hippel-Lindau disease. The Groupe Francophone d'Etude de la Maladie de von Hippel-Lindau. Gastroenterology. 2000;119:1087–1095.
44. Blansfield JA, Choyke L, Morita SY, et al: Clinical, genetic and radiographic analysis of 108 patients with von Hippel-Lindau disease (VHL) manifested by pancreatic neuroendocrine neoplasms (PNETs). Surgery. 2007;142:814–818.
45. Cives M, Strosberg J. The expanding role of somatostatin analogs in gastroenteropancreatic and lung neuroendocrine tumors. *Drugs*. 2015;75: 847-858.
46. Jiao Y, Shi C, Edil BH, et al. DAXX/ ATRX, MEN1, and mTOR pathway genes are frequently altered in pancreatic neuroendocrine tumors. *Science*. 2011;331:1199-1203.
47. Scarpa A, Chang DK, Nones K, et al. Whole-genome landscape of pancreatic neuroendocrine tumours. *Nature*. 2017;543:65-71.
48. Terris B, Scoazec JY, Rubbia L, et al. Expression of vascular endothelial growth factor in digestive neuro-endocrine tumours. *Histopathology*. 1998;32:133-138.
49. Oberg K, Casanovas O, Castano JP, et al. Molecular pathogenesis of neuro-endocrine tumors: implications for current and future therapeutic approaches. *Clin Cancer Res.* 2013;19:2842-2849.
50. Asa SL. Pancreatic endocrine tumors. *Mod Pathol.* 2011;24(2):S66-S77.
51. Hill JS, McPhee JT, McDade TP, et al: Pancreatic neuroendocrine tumors: the impact of surgical resection on survival. Cancer 2009; 115:741–751.
52. La Rosa S, Klersy C, Uccella S, et al: Improved histologic and clinicopathologic criteria for prognostic evaluation of pancreatic endocrine tumors. Hum Pathol 2009;40:30– 40.

53. Bettini R, Partelli S, Boninsegna L, et al: Tumor size correlates with malignancy in nonfunctioning pancreatic endocrine tumor. Surgery 2011;150:75–82.
54. Kvols LK, Moertel CG, O'Connell MJ, Schutt AJ, Rubin J, Hahn RG. Treatment of the malignant carcinoid syndrome. Evaluation of a long-acting somatostatin analogue. *N Engl J Med.* 1986;315:663-666.
55. Rinke A, Muller HH, Schade-Brittinger C, et al. PROMID Study Group. Placebo-controlled, double-blind, prospective, randomized study on the effect of octreotide LAR in the control of tumor growth in patients with metastatic neuroendocrine midgut tumors: a report from the PROMID Study Group. *J Clin Oncol.* 2009;27:4656-4663.
56. Caplin ME, Pavel M, Cwikla JB, et al. Lanreotide in metastatic enteropancreatic neuroendocrine tumors. *N Engl J Med.* 2014;371:224-233.
57. Yao JC, Shah MH, Ito T, et al. Everolimus for advanced pancreatic neuroendocrine tumors. *N Engl J Med.* 115. 2011;364:514-523.
58. Raymond E, Dahan L, Raoul JL, et al. Sunitinib malate for the treatment of pancreatic neuroendocrine tumors. *N Engl J Med.* 2011;364:501-513.
59. D'Onofrio M, Capelli P, Pederzoli P, editors. Imaging and pathology of pancreatic neoplasms. Milan: Springer-Verlag; 2015. pp. 1-102.
60. D'Onofrio M, Capelli P, Pederzoli P, editors. Imaging and pathology of pancreatic neoplasms. Milan: Springer-Verlag; 2015. pp. 103-194.
61. De Robertis R, D'Onofrio M, Zamboni G, et al. Pancreatic neuroendocrine neoplasms: clinical value of diffusion-weighted imaging. Neuroendocrinology. 2016;103:758-770.
62. Bakir B, Salmaslioğlu A, Poyanli A, Rozanes I, Acunas B. Diffusion weighted MR imaging of pancreatic islet cell tumors. Eur J Radiol. 2010;74:214–220.
63. Brenner R, Metens T, Bali M, Demetter P, Matos C. Pancreatic neuroendocrine tumor: added value of fusion of T2-weighted imaging and high b-value diffusion-weighted imaging for tumor detection. Eur J Radiol. 2012;81:e746–e749.

64. Schmid-Tannwald C, Schmid-Tannwald CM, Morelli JN, et al. Comparison of abdominal MRI with diffusion- weighted imaging to 68 Ga-DOTATATE PET/CT in detection of neuroendocrine tumors of the pancreas. Eur J Nucl Med Mol Imaging. 2013;40:897–907.
65. Wang Y, Chen ZE, Nikolaidis P, et al. Diffusion-weighted magnetic resonance imaging of pancreatic adenocarcinomas: association with histopathology and tumor grade. J Magn Reson Imaging. 2011;33:136-142.
66. Muraoka N, Uematsu H, Kimura H, et al. Apparent diffusion coefficient in pancreatic cancer: characterization and histopathological correlations. J Magn Reson Imaging. 2008;27:1302-1308.
67. Rosenkrantz AB, Matza BW, Sabach A, Hajdu CH, Hindman N. Pancreatic cancer: lack of association between apparent diffusion coefficient values and adverse pathological features. Clin Radiol. 2013;68:e191-e197.
68. Legrand L, Duchatelle V, Molinié V, Boulay-Coletta I, Sibileau E, Zins M. Pancreatic adenocarcinoma: MRI conspicuity and pathologic correlations. Abdom Imaging. 2015;40:85-94.
69. Hayano K, Miura F, Amano H, et al. Correlation of apparent diffusion coefficient measured by diffusion weighted MRI and clinicopathologic features in pancreatic cancer patients. J Hepatobiliary Pancreat Sci. 2013;20:243-248.
70. Fukukura Y, Takumi K, Higashi M, et al. Contrast-enhanced CT and diffusion weighted MR imaging: performance as a prognostic factor in patients with pancreatic ductal adenocarcinoma. Eur J Radiol 2014;83:612-619.
71. Lotfalizadeh E, Ronot M, Wagner M, et al. Prediction of pancreatic neuroendocrine tumour grade with MR imaging features: added value of diffusion-weighted imaging. Eur Radiol. 2017;27(4):1748-1759.
72. Guo C, Chen X, Xiao W, Wang Q, Sun K, Wang Z (2017) Pancreatic neuroendocrine neoplasms at magnetic resonance imaging: Comparison between grade 3 and grade 1/2 tumors. Onco Targets Ther 10:1465–1474.

73. De Robertis R, Cingarlini S, Tinazzi Martini P, et al. Pancreatic neuroendocrine neoplasms: Magnetic resonance imaging features according to grade and stage. World J Gastroenterol. 2015;23(2):275–285.
74. Gillies RJ, Kinahan PE, Hricak H. Radiomics: images are more than pictures, they are data. Radiology. 2016;278(2):563-577.
75. Wibmer A, Hricak H, Gondo T, et al. Haralick texture analysis of prostate MRI: utility for differentiating non-cancerous prostate from prostate cancer and differentiating prostate cancers with different Gleason scores. Eur Radiol 2015;25(10):2840–2850.
76. Coroller TP, Grossmann P, Hou Y, et al. CT based radiomic signature predicts distant metastasis in lung adenocarcinoma. Radiother Oncol 2015;114(3):345–350.
77. Yachida S, Jones S, Bozic I, et al. Distant metastasis occurs late during the genetic evolution of pancreatic cancer. Nature 2010; 467(7319):1114–1117.
78. Gerlinger M, Rowan AJ, Horswell S, et al. Intratumor heterogeneity and branched evolution revealed by multiregion sequencing. N Engl J Med 2012;366(10):883–892.
79. Sottoriva A, Spiteri I, Piccirillo SG, et al. Intratumor heterogeneity in human glioblastoma reflects cancer evolutionary dynamics. Proc Natl Acad Sci U S A 2013;110(10): 4009–4014.
80. Sequist LV, Waltman BA, Dias-Santagata D, et al. Genotypic and histological evolution of lung cancers acquiring resistance to EGFR inhibitors. Sci Transl Med 2011;3(75):75ra26.
81. De Sousa E Melo f, Vermeulen L, Fessler E, Medema JP. Cancer Heterogeneity – a multifaceted view. EMBO Rep. 2013;14(8):686-695.
82. Padhani AR. Dynamic contrast-enhanced MRI in clinical oncology: current status and future directions. J Magn Reson Imaging. 2002; 16(4):407-422.
83. Peng SL, Chen CF, Liu HL, et al. Analysis of parametric histogram from dynamic contrast-enhanced MRI: application in evaluating brain tumor response to radiotherapy. NMR Biomed. 2012; 26:443-450.
84. Downey K, Riches SF, Morgan VA, et al. Relationship between imaging biomarkers of stage I cervical cancer and poor-prognosis histologic

features: quantitative histogram analysis of diffusion-weighted MR images. AJR Am J Roentgenol. 2013;200(2):314-320.

85. Just N. Histogram analysis of the microvasculature of intracerebral human and murine glioma xenografts. Magn Reson Med. 2011;65:778-789.
86. Baek HJ, Kim HS, Kim N, Choi YJ, Kim YJ. Percent change of perfusion skewness and kurtosis: a potential imaging biomarker for early treatment response in patients with newly diagnosed glioblastomas. Radiology. 2012;264(3):834-843.
87. Song YS, Choi SH, Park CK, et al. True progression versus pseudoprogression in the treatment of glioblastoma: a comparison study of normalized cerebral blood volume and apparent diffusion coefficient by histogram analysis. Korean J Radiol. 2013;14(4):662-672.
88. Chandarana H, Rosenkrantz AB, Mussi TC, et al. Histogram analysis of whole-lesion enhancement in differentiating clear cell from papillary subtype of renal cell cancer. Radiology. 2012;265(3):790-798.
89. Woo S, Cho JY, Kim SY, Kim SH. Histogram analysis of apparent diffusion coefficient map of diffusion-weighted MRI in endometrial cancer: a preliminary correlation study with histological grade. Acta Radiol. 2014;55(10):1270-1277.
90. Chang YC, Huang CS, Liu YJ, Chen JH, Lu YS, Tseng WY. Angiogenic response of locally advanced breast cancer to neoadjuvant chemotherapy evaluated with parametric histogram from dynamic contrast-enhanced MRI. Phys Med Biol. 2004;49(16):3593-602.
91. Wen Q, Jalilian L, Lupo JM, et al. Comparison of ADC metrics and their association with outcome for patients with newly diagnosed glioblastoma being treated with radiation therapy, temozolomide, erlotinib and bevacizumab. J Neurooncol. 2015 Jan;121(2):331-339.
92. Foroutan P, Kreahling JM, Morse DL, et al. Diffusion MRI and novel texture analysis in osteosarcoma xenotransplants predicts response to anti-checkpoint therapy. PLoS One. 2013;8(12):e82875.

93. Tozer DJ, Jäger HR, Danchaivijitr N, et al. Apparent diffusion coefficient histograms may predict low-grade glioma subtype. NMR Biomed. 2007;20(1):49-57.
94. Zou X, Luo Y, Li Z, et al. Volumetric Apparent Diffusion Coefficient Histogram Analysis in Differentiating Intrahepatic Mass-Forming Cholangiocarcinoma From Hepatocellular Carcinoma. J Magn Reson Imaging. 2018 Sep 12. doi: 10.1002/jmri.26253. [Epub ahead of print].
95. Rosenkrantz A. Histogram-based apparent diffusion coefficient analysis: an emerging tool for cervical cancer characterization? AJR Am J Roentgenol. 2013;200(2):311–313.
96. Nowosielski M, Recheis W, Goebel G, et al. ADC histograms predict response to anti-angiogenic therapy in patients with recurrent high-grade glioma. Neuroradiology. 2011;53(4):291-302.
97. Kyriazi S, Collins DJ, Messiou C, et al. Metastatic ovarian and primary peritoneal cancer: assessing chemotherapy response with diffusion-weighted MR imaging--value of histogram analysis of apparent diffusion coefficients. Radiology. 2011;261(1):182-192.
98. Meyer HJ, Leifels L, Hamerla G, Höhn AK, Surov A. ADC-histogram analysis in head and neck squamous cell carcinoma. Associations with different histopathological features including expression of EGFR, VEGF, HIF-1α, Her 2 and p53. A preliminary study. Magn Reson Imaging. 2018 Dec;54:214-217.
99. Meyer HJ, Höhn A, Surov A. Histogram analysis of ADC in rectal cancer: associations with different histopathological findings including expression of EGFR, Hif1-alpha, VEGF, p53, PD1, and KI 67. A preliminary study. Oncotarget. 2018;9(26):18510-18517.
100. Sidhu HS, Benigno S, Ganeshan B, et al. Textural analysis of multiparametric MRI detects transition zone prostate cancer. Eur Radiol. 2017;27(6):2348-2358.
101. Wasif N, Ko CY, Farrell J, et al. Impact of tumor grade on prognosis in pancreatic cancer: should we include grade in AJCC staging? Ann Surg Oncol. 2010;17(9):2312-2320.

102. DeLong ER, DeLong DM, Clarke-Pearson DL. Comparing the areas under two or more correlated receiver operating characteristic curves: a nonparametric approach. Biometrics. 1998;44(3):837-845.
103. Pereira JA, Rosado E, Bali M, Metens T, Chao SL. Pancreatic neuroendocrine tumors: correlation between histogram analysis of apparent diffusion coefficient maps and tumor grade. Abdom Imaging 2015;40(8):3122-3128.
104. Nguyen HT, Shah ZK, Mortazavi A, et al. Non-invasive quantification of tumour heterogeneity in water diffusivity to differentiate malignant from benign tissues of urinary bladder: a phase I study. Eur Radiol. 2017;27:2146-2152.
105. Davnall F, Yip CS, Ljungqvist G, Selmi M, Ng F, Sanghera B. Assessment of tumor heterogeneity: an emerging imaging tool for clinical practice? Insights Imaging. 2012;3(6):573–589.
106. Ma X, Zhao X, Ouyang H, Sun F, Zhang H, Zhou C. Quantified ADC histogram analysis: a new method for differentiating mass-forming focal pancreatitis from pancreatic cancer. Acta Radiol. 2014;55(7):785-792.
107. Shindo T, Fukukura Y, Umanodan T, et al. Histogram Analysis of Apparent Diffusion Coefficient in Differentiating Pancreatic Adenocarcinoma and Neuroendocrine Tumor. Medicine (Baltimore). 2016;95(4):e2574.
108. Hoffman DH, Ream JM, Hajdu CH, Rosenkrantz AB. Utility of whole-lesion ADC histogram metrics for assessing the malignant potential of pancreatic intraductal papillary mucinous neoplasms (IPMNs). Abdom Radiol (NY). 2017;42(4):1222-1228.